EUROfusion

WPMAG-PR(17) 18545

K Yagotyntsev et al.

AC loss, inter-strand resistance and mechanical properties of prototype EU DEMO TF conductors up to 30,000 load cycles

Preprint of Paper to be submitted for publication in
Superconductor Science and Technology

This work has been carried out within the framework of the EUROfusion Consortium and has received funding from the Euratom research and training programme 2014-2018 under grant agreement No 633053. The views and opinions expressed herein do not necessarily reflect those of the European Commission.

AC loss, inter-strand resistance and mechanical properties of prototype EU DEMO TF conductors up to 30,000 load cycles

K. Yagotintsev, A. Nijhuis

[1] University of Twente, Faculty of Science & Technology, 7522 NB Enschede, The Netherlands

Abstract

Two prototype Nb_3Sn cable-in-conduit (CICC) conductors were designed and manufactured for the Toroidal Field (TF) magnet system of the envisaged European DEMO fusion reactor. The AC loss, contact resistance and mechanical properties of two sample conductors were tested in the Twente Cryogenic Cable Press under cyclic load up to 30,000 cycles. Though both conductors were designed to operate at 82 kA in a background magnetic field of 13.6 T, they reflect a different approach with respect to the magnet winding pack assembly. The first approach is based on React & Wind (RW) technology while the second is the more common Wind & React (WR) technology. Each conductor was tested first on AC loss with minimum possible handling. The impact of Lorentz load during magnet operation was simulated using the cable press. In the press each conductor specimen was subjected to transverse cyclic load up to 30,000 cycles in liquid helium bath at 4.2 K. Here a summary of results for AC loss, contact resistance, conductor deformation, mechanical heat production and conductor stiffness evolution during cycling of the load is presented. Both conductors showed similar mechanical behaviour but quite different AC loss. In comparison with previously tested ITER TF conductors, both DEMO TF conductors possess very low contact resistance resulting in high coupling loss. At the same time, load cycling has limited impact on properties of DEMO TF conductors in comparison with ITER TF conductors.

1. Introduction

The foreseen DEMO reactor is expected to be the first thermonuclear device that will produce electricity at commercial competitive cost level. The magnet system will experience hundreds of thousands of load cycles during its lifetime. At the present stage the European R&D activities include both low and high temperature superconductors as an option for the toroidal field coils in the DEMO reactor [3]. The magnet system requirements for the DEMO reactor are provided by the system code PROCESS [4] and described in [5].

Two Toroidal Field (TF) conductors manufactured by routes proposed by Swiss Plasma Center (CH) and ENEA (IT) were tested at the University of Twente. Both sample conductors use Nb_3Sn superconducting technology with forced He flow as a coolant. The conductor's design is described in detail in [1,2,6]. One of the major differences between the conductors is the different approach of the magnet system winding. The sample made by SPC is based on the React & Wind (RW) concept indicated as Winding Pack 1 (WP1) while the sample from ENEA uses the more conservative Wind & React (WR) route, referred to as WP2. The sample specifications are given in Table 1.

Conductor specimens were delivered to University of Twente for the AC loss and cyclic load tests. The cyclic load test simulates the impact of Lorentz force on the conductor during magnet operation. During magnet operation, the large Lorentz force results in several effects with AC coupling loss change, strand deformation, formation of a gap between conduit and strands bundle [7] and strand motion and hence mechanical heat generation [8,9] as most important phenomena. Since the electromagnetic load in the DEMO magnet system has a cyclic nature, knowledge of electrical and mechanical properties of conductors as a function of cyclic load is essential to understand and determine the conductor performance over the magnet lifetime.

The evolution of AC loss, contact resistances and mechanical properties were recorded as a function of load cycle number. In addition, separate conductor specimens with minimum possible handling (virgin state) were tested on AC loss by calorimetry for direct comparison and calibration. The calorimetric measurements done on the virgin samples were performed with the field orientation parallel and perpendicular to the conductor wide plane..

	RW WP1 (React & Wind)	WR WP2 (Wind & React)
SC strands number	306	1080
Strand diameter (mm)	1.5	1.0
Cu strands	17 (1.5 mm diam.)	132 (1.5 mm diam.)
Non-cu J_{op} (A/mm^2)(A/mm^2)	298.7	192.6
Final cable layout	(1Cu + 6 + 12) x 17	(4 type-I petals + 2 type-II petals) around core2 (core2, with Cu: 3x4x(6+1))*
Cable height x width (mm)		

Designed void fraction (%)	19.0	24.6

Table 1. Sample specification.

* petals type-I are around Cu core, petals type-II are around cooling spiral.

2. Experimental setups and sample preparation

The AC loss of the virgin state samples is measured in the AC dipole setup [10]. The setup provides AC and DC magnetic field with an accelerator field quality homogeneous field length of 50 cm. The measurement is carried out at 4.2 K in liquid He bath with a sinusoidal modulation field of ±0.15 T amplitude with and without an offset field of 0.35 T. The applied magnetic field frequency range is 1 to 155 mHz. The dipole magnet is equipped with a calorimeter that is inserted in the bore of the magnet. The power dissipation of the sample is measured by means of a calibrated gas flow of helium boil off. Besides the calorimetric measurement, magnetisation $M(B)$ loops are obtained with a set of compensated pick-up coils wound around the conductor. The virgin state samples are equipped with two pick-up coil sets that are perpendicular oriented to each other in order to measure magnetisation loss for perpendicular and parallel field orientations. Perpendicular orientation means that the applied magnetic field is oriented perpendicular to the wide side of the conductor while in parallel orientation the magnetic field is parallel with the wide side of the conductor. The measured AC loss is normalized per volume of superconducting Nb_3Sn strands. The sample volume is calculated as the conductor length multiplied by superconducting strand number and strand cross section. The volume is 216.6 cm^3 for the RW sample and 339.3 cm^3 for WR. The magnetization loop area is calibrated against the simultaneously measured calorimetric data by using a multiplicative factor. The multiplicative factor is constant for all frequency range.

The second set of samples is used in the Twente cryogenic cable press to study the evolution of the AC loss and mechanical properties of conductor specimens as a function of cyclic load. The design of the cryogenic press is described in detail in [11]. The press was previously used to test various types of NbTi and Nb_3Sn cable in conduit conductors (CICC) [12-17]. The sample position in the press gap is such that the press applies force perpendicular to the wide side of the sample, i.e. similar to the Lorentz force during magnet operation. The transverse displacement is measured by a set of calibrated displacement meters attached to the conductor jacket halves. The load applied to the sample is measured by a load cell and by a set of calibrated strain gauges, which measure the deformation of the press stamp. The press is equipped with a superconducting dipole magnet in order to study

the AC loss evolution with load cycle number. The dipole magnet generates a magnetic field perpendicular to the wide side of the press sample. The AC loss in the press is measured by magnetisation method only. To calibrate the magnetisation loops obtained in the press we assume that prior to any load (initial conductor condition), the sample state in the press is identical to the one measured in the virgin state condition in the AC dipole setup and the same calibration factor is used for all following cycles.

The peak electromagnetic load on the DEMO TF conductor during magnet operation is 1076 kN/m (B=13.06 T, I=82.4 kA) [5]. The stress distribution in the conductor differs for the press case with respect to the magnet conditions. The peak Lorentz force is accumulated through the strand layers in the conductor while in the cryogenic press a uniform pressure is applied. The average stress in the cable for Lorentz force is half the peak force (BxI) [8,9]. Hence, the upper limit of the transverse peak load in the press was set to 538 kN/m to have a representative transverse load with respect to the interstrand contact resistance and coupling loss during mechanical cycling of the load.

The measurements in the press are done at 4.2 K in liquid He bath during one cool down session without interruption . The magnetization, inter strand contact resistance and force-displacement are monitored during the cyclic load test at initial state, cycle number 1, 2, 10, 100, 1,000, 3,000, 10,000, 20,000 and 30,000. At each selected load cycle, the AC loss is measured in fully unloaded state and in fully loaded state. Under fully unloaded state the sample is allowed to relax while its maximum relaxation is restricted to the initial CICC dimensions by the limited void fraction method [14]. After each cycle, sufficient time is taken for stabilisation of time relaxation effects.

The contact resistance, R_c, is measured by selecting pairs of superconducting strands from the cable and performing a four-point measurement with a current of 50 A. No influence of the DC background magnetic field on the contact resistance was observed for both samples, and thus the contact resistances were measured without background magnetic field.

2.1. Sample preparation RW WP1

For the RW React and Wind approach the cable was delivered without conduit and outer copper stabilizing strands so stainless steel jackets were manufactured for virgin and press samples. The conductor was fixed at the both ends to avoid changes in twist pitch lengths.. The 316L alloy jackets were made with inner dimensions of 11.9 x 62.1 mm corresponding to the cable dimensions according to the conductor specification [1,6]. The jacket halves of the sample for the AC dipole test were spot welded together with temperature control. The press sample jacket halves were fixed together by bolts. After

jacketing both samples were heat treated. The samples were cut by spark erosion to their final length of 400 mm after heat treatment.

The RW conductor as delivered did not have the stainless steel strip in the center of the conductor as foreseen in the original design since it got lost during the manufacture of the cable. The additionally delivered stainless steel strip was fit inside the virgin and press RW samples before heat treatment. After heat treatment the internal dimensions of the conductor jacket were 11.85 x 62.1 mm for both samples. Figure 1 shows the cross section of RW and WR virgin AC loss samples.

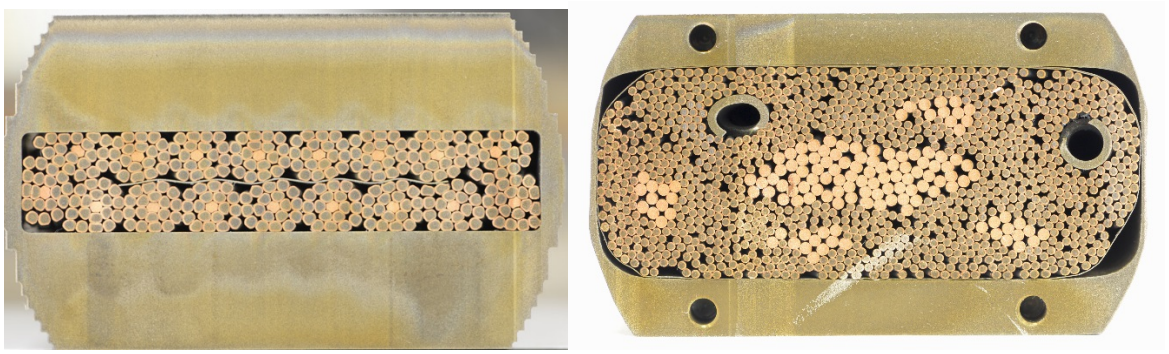

Figure 1. Cross sections of samples prepared for AC loss measurement in virgin condition. RW WP1 (left) and WR WP2 (right).

For the press sample, a slit of 2 mm width was foreseen to separate the conductor jacket halves along the sample length in order to allow free cable compression under transverse load. The jacket halves were secured with bolts but allowing free cable compression and at the same time restricting the conductor expansion beyond the specified conductor dimension (locked void-fraction method [14]). A set of pick-up and compensating coils for AC loss measurement by sample magnetisation was mounted on the press sample. The pick-up and compensating coils are attached to the same conductor jacket halve, to make sure that during load cycling the relative position of the coils remains the same. For the measurement of mechanical compression and relative jacket halves displacement, the sample is instrumented with a set of six displacement meters, which are bending beams with strain gauges. Adjacent to each of these displacement meters, a quartz rod-in-tube is attached to a micrometer differentially in order to calibrate the displacement meters.
In total 20 strands are selected for contact resistance measurements.

Figure 2 and Figure 3 show the scheme of strands selection for RW and WR conductors with four different strands combinations R_{c1} – R_{c4} for the intra-petal R_c measurements of the RW sample. The presented R_c value for each strand combination is the average value between at least two strands (except R_{c3}) in equivalent positions (see Figure 2 and Table 2). Two strands were selected from petals P2 – P9 of the RW conductor for the inter-petal R_c measurement. Strands are selected in such a way that one strand is part of the inner layer of the petal and the second strand is taken from the outer layer in order to find a representative average inter-petal value. Petals P10 - P17 were excluded from R_c measurement because of the conductor symmetry. The combinations of strands are summarized in Table 2. The selected strands are mounted on a support plate attached to the conductor jacket and the remaining strands were cut. The sample was heat treated in vacuum and Figure 4 shows the RW press sample fully prepared for testing.

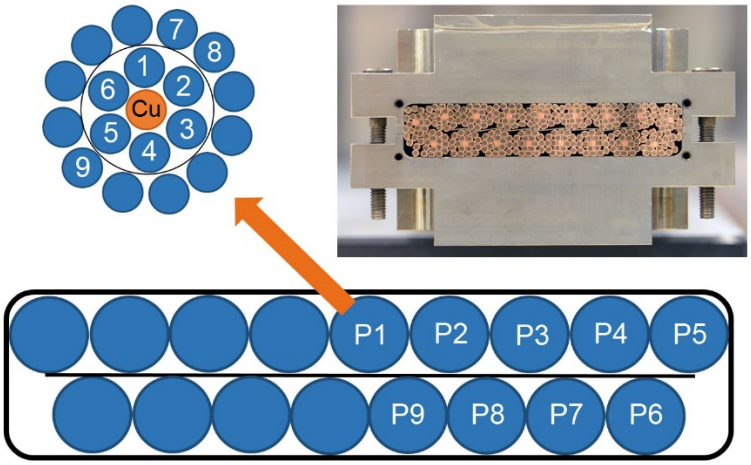

Figure 2. Scheme of the strand selection for contact resistance measurement and cross section of the press sample.

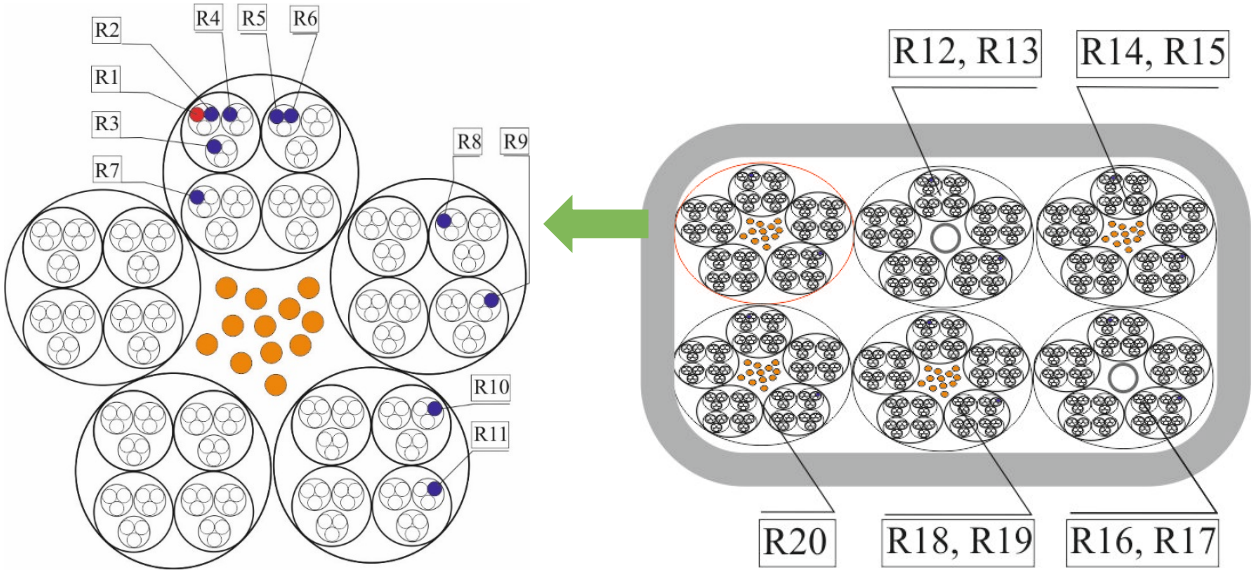

Figure 3. Scheme of the strand selection for contact resistance measurement.

Table 2. Strand combinations for contact resistance measurement.

R_{st} combination / petal	Strand combinations
R_{st1} (intra-petal, petal 1)	R1-R2; R1-R6
R_{st2} (intra-petal, petal 1)	R1-R3; R1-R5
R_{st3} (intra-petal, petal 1)	R1-R4
R_{st4} (intra-petal, petal 1)	R1-R7; R1-R8; R1-R9
petal 2 (inter-petal)	R1- R10; R1- R11
petal 3 (inter-petal)	R1- R12; R1- R14
petal 4 (inter-petal)	not selected
petal 5 (inter-petal)	R1- R14; R1- R15
petal 6 (inter-petal)	not selected
petal 7 (inter-petal)	R1- R16
petal 8 (inter-petal)	R1- R17; R1- R18
petal 9 (inter-petal)	R1- R19; R1- R20

Table 3. Strand combinations for contact resistance measurement.

R_{st} combination / petal	Strand combinations
R_{st1} 1st stage (intra-petal)	R1–R2; R5–R6

R_{st2} 2nd stage (intra-petal)	R1–R3; R1–R4
R_{st3} 3rd stage (intra-petal)	R1–R5; R1–R6; R1–R7
R_{st4} 4th stage (intra-petal)	R1–R8; R1–R9
R_{st5} 5th stage (intra-petal)	R1–R10; R1–R11
petal 2 (inter-petal)	R1–R12; R1–R13
petal 3 (inter-petal)	R1–R14; R1–R15
petal 4 (inter-petal)	R1–R16; R1–R17
petal 5 (inter-petal)	R1–R18; R1–R19
petal 6 (inter-petal)	R1–R20

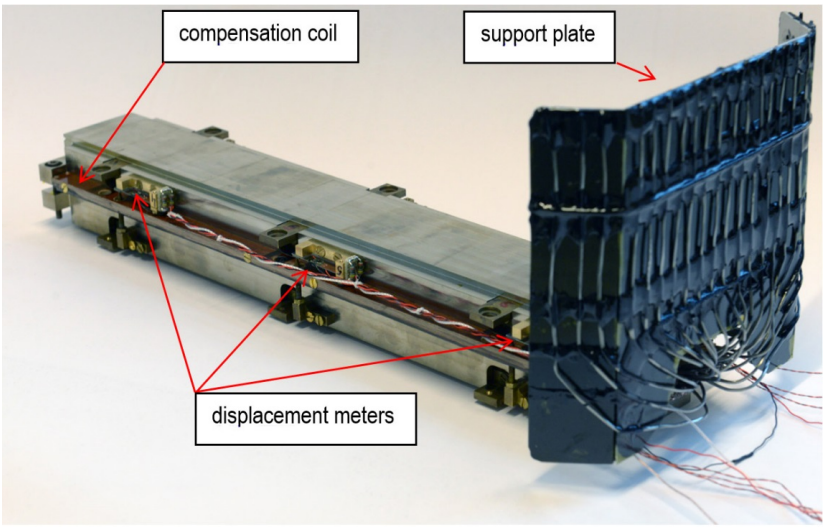

Figure 4. Fully prepared RW WP1 press sample.

2.2. WR WP2 sample

The WR sample is having a stainless steel conductor conduit of ~6.6 mm wall thickness. The thickness of the conduit side walls had to be reduced for the virgin sample in order to fit in the dipole calorimeter, no other modification was made to the sample. The sample was clamped during heat treatment to avoid changes in the conductor dimensions because of the thin conduit walls. After heat treatment the sample was cut by spark erosion to its final length of 400 mm. Figure 1 shows the cross section of the sample prepared for AC loss measurement in the dipole. For the press sample, a slit of ~5 mm width was made in the conductor conduit at both sides along the sample length in order to allow compression of the cable under transverse load. For the inter strand contact resistance measurements

the strands are selected according to the scheme shown in Figure 3. For the intra-petal R_c measurements strands were selected in such a way that each cabling stage is represented by at least two strand combinations. The R_c value of a given cabling stage is the average value measured for strands in equivalent positions. The combinations of strands are summarized in Table 3**Error! Reference source not found.**.

3. Experimental results

3.1. Virgin AC loss

Figure 5 shows the loss-frequency dependencies of both virgin samples for perpendicular and parallel field orientations. The agreement between the AC loss measured by calorimetry and magnetization is good for both samples while Figure 5 only presents the magnetization data for clarity.

Only a small influence of the background field on the AC loss was observed.

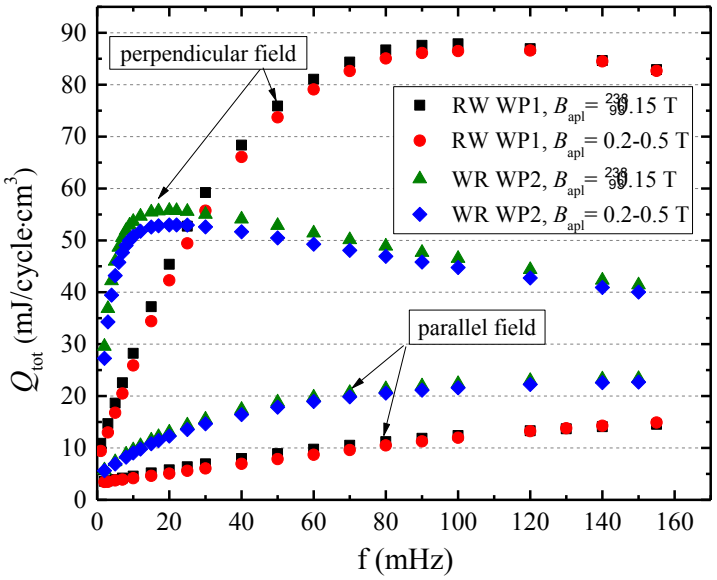

Figure 5. RW WP1 and WR WP2 virgin samples AC loss comparison for two field-conductor orientations.

The loss-frequency dependence of the measured conductors deviates from linear behaviour already at very low magnetic field frequencies. To find the initial slope of the loss

curve and offset, a 2nd order polynomial function was used to fit the RW sample data. From the fit the slopes α and constant offsets of loss – frequency curves were determined in the low frequency limit. The slope α represents coupling loss while constant offset represents hysteresis loss Q_{hys} in the conductor. The WR sample loss-frequency dependence deviates strongly from linear behaviour even at frequencies below 8 mHz, which required the use a 3rd order polynomial function for perpendicular field orientation. For the fit we used a frequency range between 1 and 60 mHz for RW and1 to 8 mHz for WR in order to stay below the AC loss peaks. For parallel field orientation, 2nd order polynomial functions covering the full frequency range were used for both samples. The coupling loss time constant $n\tau$ is based on the initial slope α [18]:

$$n\tau = \alpha \frac{\mu_0}{2\pi^2 {B_a}^2} \quad \text{(s)}, \qquad (1)$$

where B_a is the amplitude of the applied sinusoidal magnetic field.

To find the position of the AC loss peak, the data points in the vicinity of the AC loss peak are fit with a gauss function. Table 4 presents the Q_{hys}, $n\tau$ values and position of the AC loss peak for the measured DEMO TF samples in virgin condition.

Both samples have high coupling loss in virgin state; 5.8 s for RW and 34.5 s for WR with perpendicular field orientation and offset field. That is an order of magnitude higher than ITER Nb_3Sn conductors with $n\tau$ values in the range of 0.5 -1.0 s in virgin condition [17].

It was shown for ITER Nb_3Sn type conductors that the coupling time constant increases drastically with decreasing the void fraction from 24 to 21% [19]. In the case of the WR conductor, the low void fraction is even combined with the absence of resistive petal wraps. It was shown previously [14] that for a conductor without petal wraps the last stage coupling loss is dominant, in particular at the low frequency range. The high coupling loss of the WR sample in particular is due to the absence of petal wraps leading to very low inter-petal contact resistance. This is supported by the contact resistance measurement presented in section 3.3. There it is shown that the average inter-petal resistance of the WP sample is an order of magnitude less than the lowest R_c observed for ITER CS conductors while the average intra-petal resistance is in the same range as ITER CS conductors [17].

The AC loss of the WR sample was measured previously in the EDIPO facility, showing that the AC loss peak was below 40 mHz [2]. In the EDIPO measurement, no AC loss peak position and coupling time constant could be determined because the applied frequency range was above that of the AC loss peak. The measurements from Twente show

that the AC loss peak position is located at ~20 mHz for the virgin WR sample for perpendicular field orientation.

Table 4. Hysteresis loss, coupling loss time constants and AC loss peak positions for RW WP1 and WR WP2 DEMO TF conductors in virgin condition.

	perpendicular field orientation		parallel field orientation	
	RW WP1	WR WP2	RW WP1	WR WP2
	Q_{hys} (mJ/cm^3·cycle)			
B_{apl} = ± 0.15 T	8.5 ± 0.3	8.0 ± 0.1	3.2 ± 0.1	4.9 ± 0.1
B_{apl} = 0.2 - 0.5 T	7.1 ± 0.1	7.4 ± 0.2	3.2 ± 0.1	4.7 ± 0.1
	$n\tau$ (s)			
B_{apl} = ± 0.15 T	6,1 ± 0.1	37.9 ± 0.2	0.4 ± 0.01	1.4 ± 0.1
B_{apl} = 0.2 - 0.5 T	5,8 ± 0.1	34.5 ± 0.5	0.3 ± 0.01	1.3 ± 0.1
	AC loss peak position (mHz)			
B_{apl} = ± 0.15 T	100± 5	21.4 ± 0.4	-	-
B_{apl} = 0.2 - 0.5 T	100± 5	22.7 ± 0.5	-	-

3.1.1. Magnetic field angle and hysteresis loss

Table 4 shows that the hysteresis loss of both samples appears to be less with the magnetic field parallel to the wide side of the conductor compared with perpendicular orientation. It can be noted here that some Rutherford type conductors also showed different hysteresis loss for perpendicular and parallel magnetic field orientations [20] while other Rutherford conductors has the same hysteresis loss values for both field –conductor orientations [21].

In order to identify the role of the rectangular shape with respect to the amplitude of the applied sinusoidal magnetic field, the total AC loss of the WR sample was measured as function of magnetic field amplitude. The magnetisation measurements were done in the AC dipole with a magnetic field frequency of 10 mHz. The AC loss is normalized by the square of the applied magnetic field amplitude and plot versus the amplitude of the applied magnetic field in Figure 6**Error! Reference source not found.**. Although not the full range was measured for perpendicular field, AC loss saturation occurs at about 0.35 T for perpendicular orientation, while for parallel field saturation is reached around 0.55 T. Taking into account the amplitudes of applied magnetic field used for the AC loss versus frequency

measurements, it seems that the observed disparity in hysteresis loss for different field-sample orientations can only be partly justified by a difference in penetration field for altered field orientations. Another effect that is involved is the accuracy of the fit extrapolation of the total loss towards zero frequency. It can be argued that the experimental data at lower frequencies are less accurate and extrapolation with a third order polynomial is rather arbitrarily. This suggests that the actual coupling loss for perpendicular direction could even be higher than as presented here according to the followed methodology. Another effect that finally might be considered here is demagnetisation, which differs for both applied field directions due to the large dissimilarity in aspect ratio of the conductor cross sections. A larger difference would then be expected for the RW conductor and this what is actually measured.

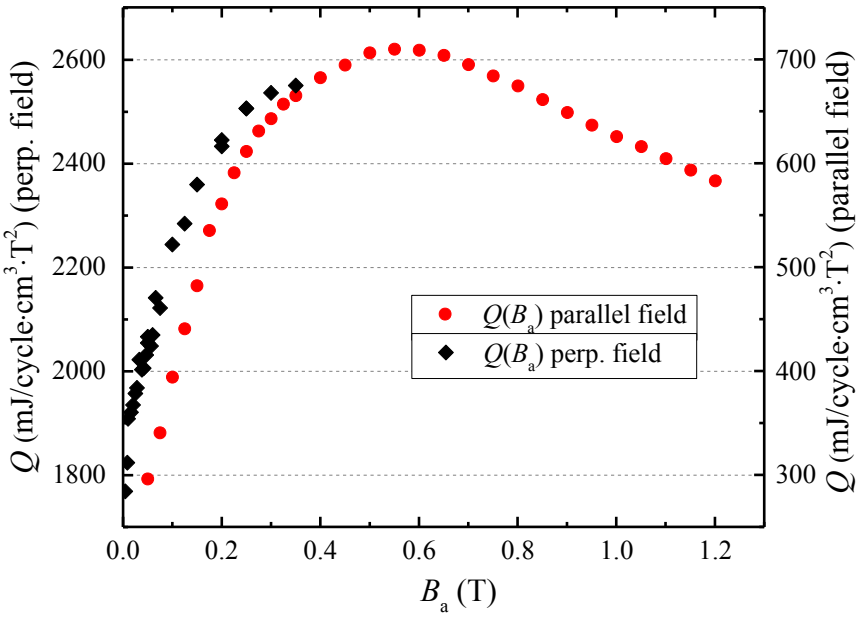

Figure 6. AC loss divided by the square of the magnetic field amplitude versus the amplitude of the sinusoidal magnetic field measured by magnetisation at a frequency of 10 mHz. The left axis represents the normalized loss for perpendicular direction, the right axis for parallel direction.

3.2. AC loss with cyclic loading

The range of magnetic field frequency used in the press setup to measure the AC loss is from 10 to 160 mHz for the RW and from 5 to 160 mHz for the WR sample. The

comparison of the initial AC loss measurement in the press setup showed that at frequencies higher than 60 mHz, the AC loss values measured in the press setup are systematically higher than for the virgin samples data. At magnetic field frequencies lower than 60 mHz both measurements were in good agreement.

Figure 7 shows the loss-frequency dependencies for the initial state press samples and after 30,000 load cycles at zero load state. The evolution of the AC loss under full load has the same behaviour though the total loss is higher due to increased coupling between strands due to lower contact resistance.

The total loss of the RW sample decreases with cycling of the load and the AC loss behaviour is similar to what is observed earlier for ITER Nb_3Sn CICCs [17]. The total loss of WR sample decreases at frequencies below the AC loss peak while at frequencies above the peak, the total loss rises with load cycle number in Figure 7. The same increase of the total loss was also observed for the WR conductor after electromagnetic load cycle in the EDIPO facility [2] though authors observed only the frequency range above the AC loss peak.

In general it is observed that an increase of contact resistance with cycle number leads to a decrease of the coupling currents. That is in agreement with the observed lower loss at the field frequencies below the AC loss peak. At the field frequencies above the AC loss peak, the internal part of the sample is partially shielded by coupling currents. It is suggested that the decrease of the coupling currents at the higher frequencies increases the volume of the sample that is involved in the AC loss energy dissipation and hence increases the total AC loss.

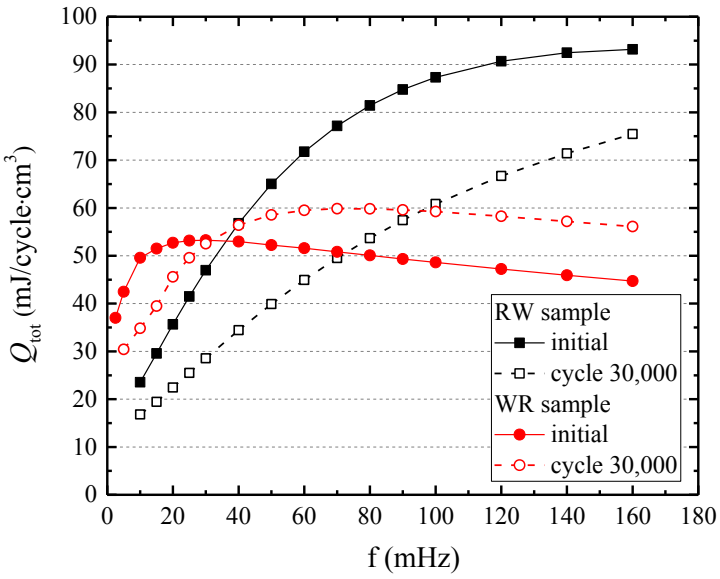

Figure 7. Loss-frequency characteristics of RW and WR samples measured in initial conditions in the press setup and at cycle 30,000 in fully unloaded state.

The AC loss peak occurred in the press at slightly higher frequencies than for the virgin samples in the dipole magnet. The position of the AC loss peak measured in the press setup is ~160 mHz for RW and at ~30 mHz for WR sample. Figure 8 illustrates how the position of the AC loss peak of the WR specimen gradually shifts toward higher frequencies with increasing number of load cycles. After 3,000 cycles, the position of the AC loss peak saturates at 70 mHz and 60 mHz for zero and full loaded sample respectively. The saturation in the AC loss peak position indicates that the main part of the changes due to the cyclic loading occurs the first 3,000 cycles. The EDIPO test showed that the AC loss peak position of the WR sample was at about 40 mHz after 1150 load cycles [2]. In the Press measurement, the AC loss peak position was observed at ~50 mHz after 1,000 load cycles, indicating that both measurements are in good agreement. We were not able to trace the evolution of the peak position with load cycles for the RW sample since the peak position is above the magnetic field frequencies used in the Press.

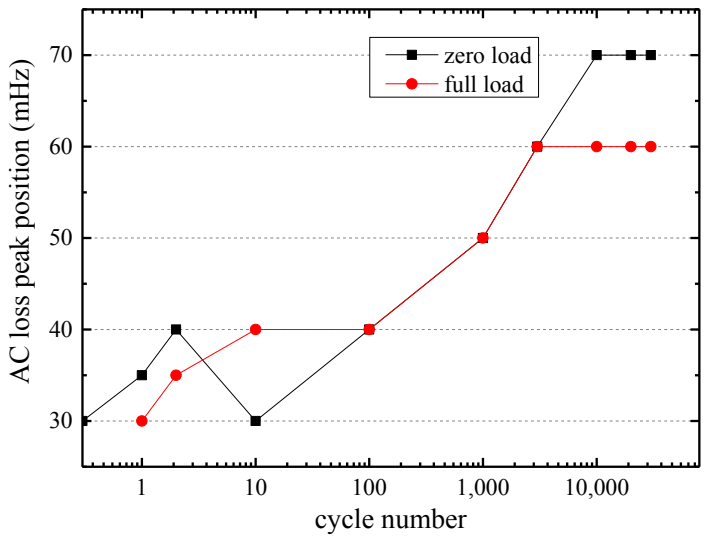

Figure 8. Evolution of AC loss peak position with load cycles for zero and full loaded samples.

Similar to the procedure followed with virgin samples, the loss-frequency dependence of each cycle was fitted by a polynomial function to find the initial loss curve slope α. Data points were included in the fit below 60 mHz for RW sample and below the AC loss peak for the WR sample. The limited number of data points below the AC loss peak in the case of the WR sample results in a relatively big error of ~20% in the fit of the slope α and hence in the coupling loss time constant $n\tau$. Extending the magnetic field frequencies to even lower frequencies (as we did in AC dipole test with virgin samples) would increase the measurement accuracy but at the same time to an inappropriate increase of experimental time. The lowest magnetic field frequency of 5 mHz was chosen as an optimum between experimental time and measurement accuracy for the WR sample.

Figure 9 and Figure 10 show the evolution of the coupling loss time constant $n\tau$ with cycle number for RW and WR samples. The initial time constant measured in the press are $n\tau$ = 4,2 ± 0.6 s for RW and 27.0 ± 4.7 s for WR. It is about 2 s and 8 s lower respectively, comparted with $n\tau$ values measured for the virgin samples in the AC dipole. Possibly, additional handling of the press samples and lower field quality in the press setup may be responsible for that difference.

When cyclic loading is started, coupling loss time constants of both samples decreases showing behaviour qualitatively similar to measured previously on ITER Nb_3Sn CICC

conductors [17]. The coupling loss is higher in the fully loaded state as the inter-strand coupling is increased due to compaction. The biggest decrease of $n\tau$ was observed during the first cycle for both samples. The main change in coupling loss take place up to 3,000 cycles for both samples. That is in good agreement with the evolution of the AC loss peak position of the WR sample and evolution of samples displacement during load cycling (see chapter 3.4). Even at the end of load cycling, the absolute $n\tau$ values stay at high level for both samples. After 30,000 load cycles, the $n\tau$ values of the RW sample are 1.8 s at zero load and 2.3 s at full load. The WR specimen has $n\tau$ values of 17.4 s at zero and 18.4 s at full load after 30,000 load cycles.

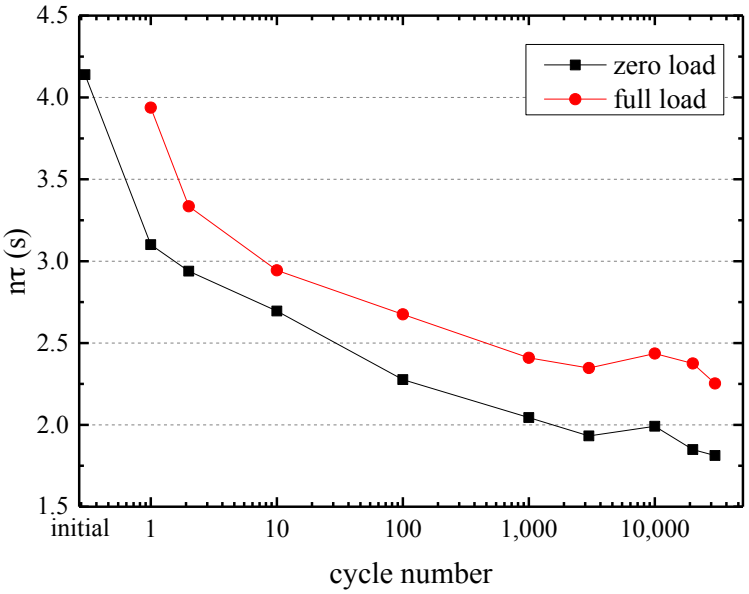

Figure 9. Evolution of coupling loss time constant nτ with number of load cycles for RW WP1 conductor.

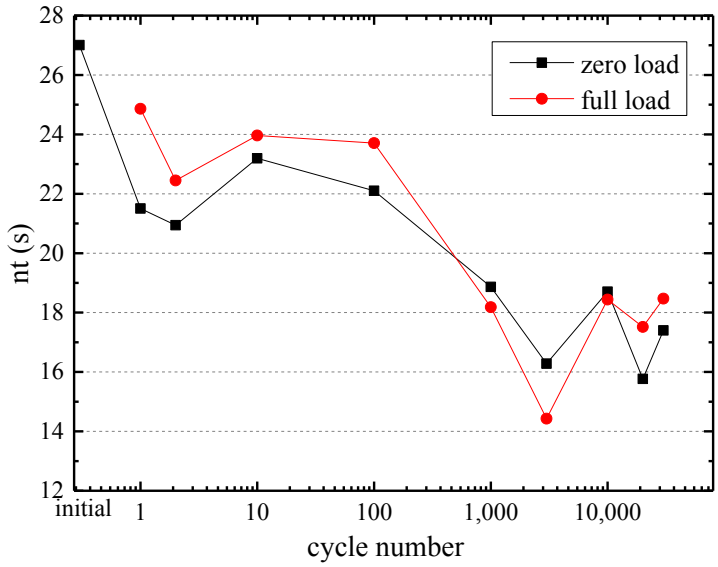

Figure 10. Evolution of coupling loss time constant nτ with number of load cycles for WR WP2 conductor.

3.3. Contact resistance measurement

3.3.1. Contact resistance versus applied load

The contact resistance between a pairs of neighbouring strands R_{st1} (see Table 2 and **Error! Reference source not found.Error! Reference source not found.**) was monitored during stepwise load increase and decrease. The evolution of R_c versus applied load and the cycle numbers is shown in Figure 11 for both samples. Prior to any load applied, the R_{st1} value is 2.5 nΩm for RW and 3.4 nΩm for WR samples. During the first load cycle, R_{st1} shows a hysteretic behaviour increasing from its initial value to 3.0 nΩm and 3.8 nΩm at the last cycle, for RW and WR samples respectively. The subsequent resistance change over the full cycle is much smaller and stays within the error bar of the measurement. As the number of cycles increases, the difference between R_{st1} at zero load and at full load also increases from less than 0.5 nΩm at cycle 2 to ~1 nΩm at cycle 30,000. The final R_{st1} value at zero load after 30,000 cycles amounts to ~6.5 nΩm for the RW sample (260 % of the initial value) and ~4.7 nΩm for the WR sample (130 % of the initial value). Cycling of the load has a higher impact on the RW than on WR conductor.

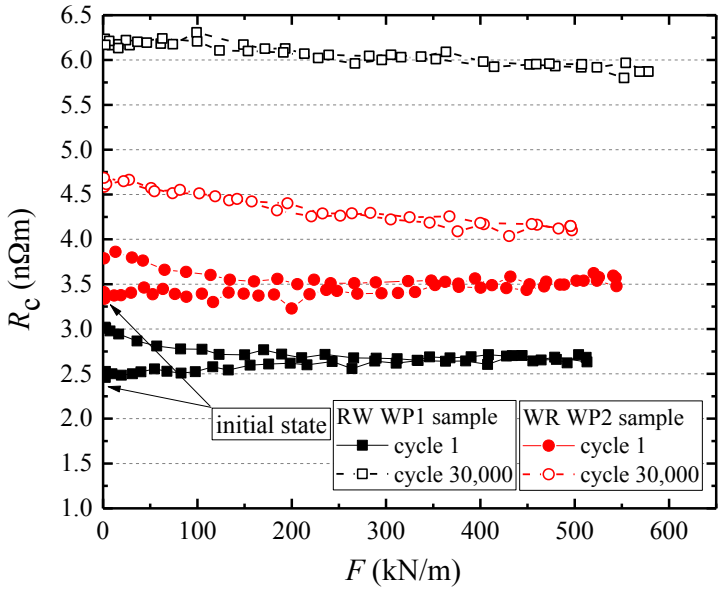

Figure 11. Evolution of R_{st1} as a function of applied load at cycles 1 and 30,000.

3.3.2. Contact resistance with cyclic loading

The contact resistance between different strand combinations within one petal (intra-petal) and also between petals (inter-petal) were measured at zero and full load as a function of cycle number. For both samples it was observed that the locations of the strand pair combination corresponds well with the values of R_c. The lowest intra-petal resistance is always observed for immediately neighbouring strands R_{st1} (line contact between strands) and the highest intra-petal resistance is observed between strand pairs selected from inner and outer ring (R_{st4} combination of RW sample) or between strands from the fifth cabling stage (R_{st5} of RW sample). Figure 12 and Figure 13 show the evolution of the average intra and inter-petal resistance at zero and full load versus cycle number for both samples. Both samples have almost similar average initial intra-petal resistance and also comparable intra-petal resistance evolution with cycling load. Both samples show about 3 nΩm increase of intra-petal resistance up to 30,000 cycles under zero and full load.

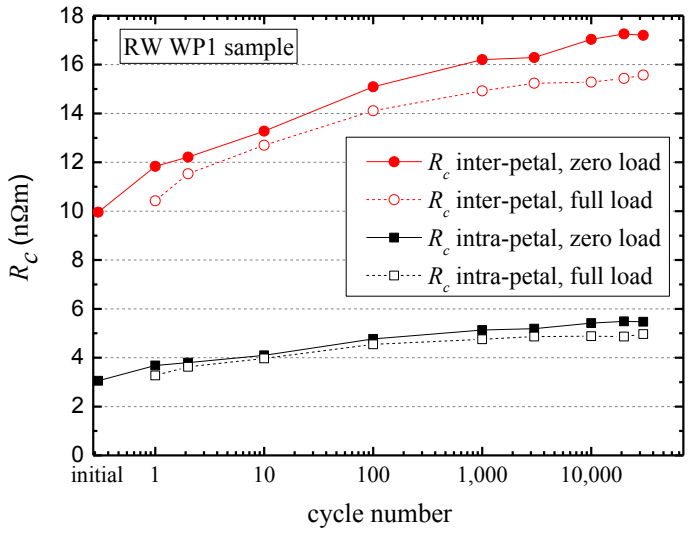

Figure 12. Intra and inter-petal resistance versus number of load cycles for RW WP1 sample.

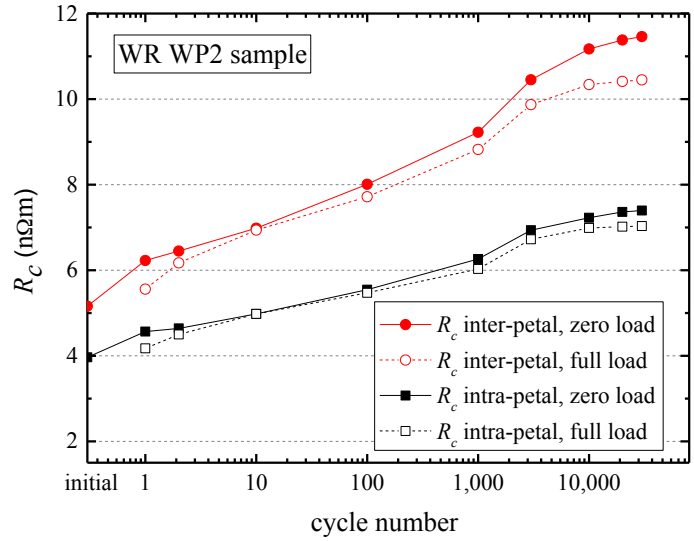

Figure 13. Intra and inter-petal resistance versus number of load cycles for WR WP2 sample.

At the initial state, the inter-petal resistance is 10.0 nΩm for the RW sample and 5.2 nΩm for the WR sample. The RW conductor shows a larger increase of the inter-petal resistance

than the WR sample. The average inter-petal resistance of the RW conductor increases from 10.0 to 17.2 nΩm while that of the WR conductor increases from 5.2 to 11.5 nΩm up to 30,000 cycles. The impact of cycling load on the intra-petal resistance is more pronounced for the RW sample.

3.4. Mechanical properties

The cable conduit halves relative displacement, *d*, is measured at each of the loading/unloading steps for the selected load cycle. Figure 14 shows displacement-force curves typical for visco-elasto-plastic deformations as observed previously in Nb_3Sn and NiTi CICC conductors [9]Figure **14.** Force –displacement curves for RW and WR DEMO samples. during cycle 1 and 30,000.

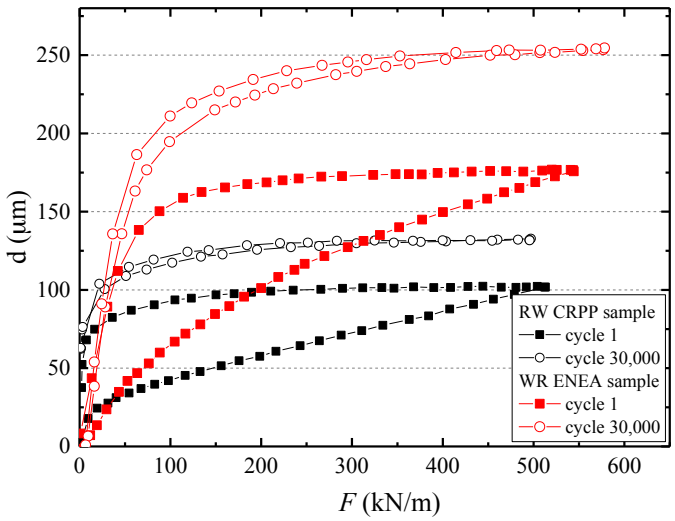

Figure 14. Force –displacement curves for RW and WR DEMO samples.

Due to small the void fraction and large aspect ratio, both samples have relatively low displacement under applied load. Figure 15 shows the evolution of the maximum displacement during cycling of the load. At the first cycle, a maximum displacement d_{max} of 102 μm is reached for the RW conductor while the WR sample has a displacement of 177 μm. The deflection of the WR sample is more since it has a larger void fraction and the size of the sample in compressive direction is about twice that of the RW sample. The

observed compaction of the DEMO TF conductors is about 8 times smaller than for the ITER TF conductors that is typically between 800 and 1250 μm at the first full load [17]. The maximum displacement of both DEMO conductors saturates after ~3,000 cycles. After 30,000 cycles, the maximum displacement becomes 133 μm for RW and 255 μm for WR.

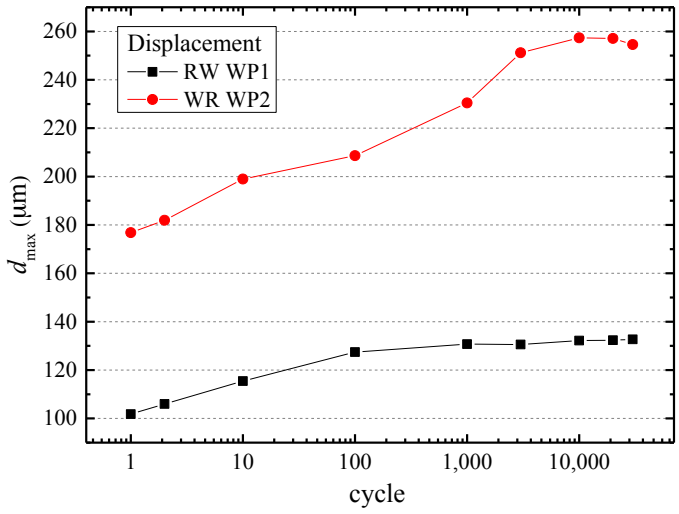

Figure 15. Maximum displacement for RW and WR DEMO TF samples under full load.

The hysteretic force-displacement curves shown in Figure 14 correspond to a mechanical loss in the conductor (Q_m) due to strand motion and deformation. The loss is calculated as the area enclosed by the hysteretic force-displacement curves:

$$Q_m = \oint F_y dy \qquad \text{(J cycle}^{-1}\text{)}, \tag{2}$$

Where F_y is the applied transverse force and d_y is the conductor transverse deformation. We normalized the mechanical loss per strand volume for both conductors in order to make a direct comparison. Figure 16 shows the evolution of the normalized mechanical loss with number of cycle load. Along the whole number of cycles, the WR conductor has higher mechanical loss than the RW sample, which corresponds well with the larger deflection rate of the WR sample. The overall mechanical loss is low and saturates after 10 cycles at the level of ~ 2 and 5 mJ/cm^3 for RW and WR samples respectively and is negligible in comparison with the AC loss. The mechanical heat production is very low compared with the level of 31 ± 4 (mJ/cycle·cm^3) typically observed for ITER TF conductors

[17]. The low heat production can be attributed to the limited strands motion due to the low void fraction in both DEMO conductors.

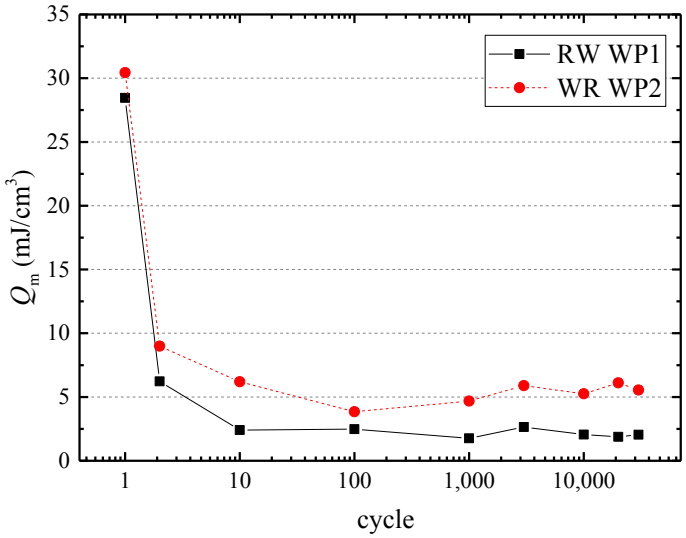

Figure 16. Mechanical loss with load cycle for RW and WR conductors.

3.5. Elastic modulus

The elastic modulus in transverse direction is evaluated from the displacement-force curves by considering the load on the longitudinal cross section of the cable. Hence, the elastic modulus E_y is:

$$E_y = \frac{DF}{A_y d} \quad \text{(Pa)}, \qquad (2)$$

where D is the cable thickness and A_y is the cable cross section area perpendicular to the applied load. For A_y, we took 0.025 m^2 area for the RW WP1 sample and 0.027 m^2 for the WR WP2. The overall behaviour of the elastic modulus versus applied load is consistent with that observed earlier for ITER Nb_3Sn conductors. Figure 17 shows the evolution of the elastic modules versus cycle number. When cycling of the load is started, the elastic modules at maximum load start to decrease gradually for both samples. After 1,000 load cycles the RW sample reaches saturation and E_y stays at the level of 2.0 GPa at full load. The elastic modulus of the WR WP2 conductor reaches saturation after 3,000 load cycles with the same saturation value of 2.0 GPa at maximum load. During load increase, the E_y of

both samples increases from zero in fully unloaded state to its maximum almost linearly (except for the first cycle) with applied load, upon release of the load the same linear behaviour is observed.

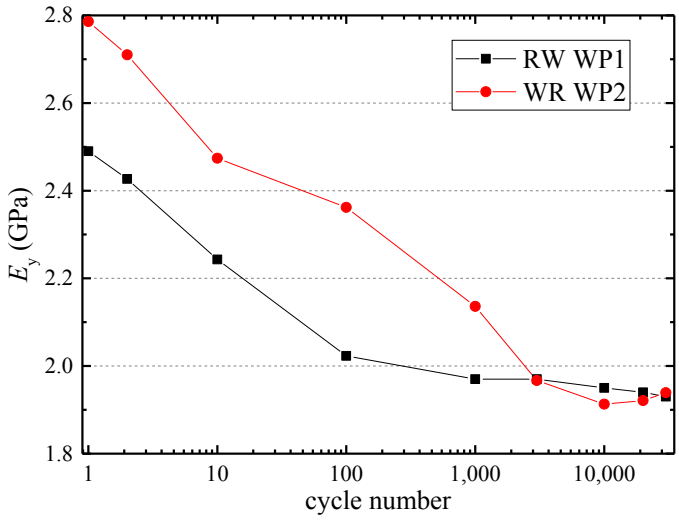

Figure 17. Comparison of E_y at maximum load versus cycle number for RW and WR samples.

The conductor stiffness at a certain level of stress is defined by the dynamic elastic modulus [9]**Error! Reference source not found.** by differentiating E_y with respect to the displacement such that:

$$\frac{\delta\sigma}{\delta\varepsilon} = \frac{D}{A_y}\frac{\partial F}{\partial d} \quad \text{(Pa)}, \qquad (3)$$

At the first cycle during loading, $\delta\sigma/\delta\varepsilon$ remains around 3 GPa for both conductors as the major part of the deformation takes place on the first cycle through strand movement. From cycle 2, $\delta\sigma/\delta\varepsilon$ follows the same trajectory reaching ~40 GPa for the RW sample and ~30 GPa for the WR sample at full load in Figure 18. The dynamic elastic modulus measured for the DEMO conductors is similar to that measured earlier for ITER TF (30 - 40 GPa at a load of 517 kN/m) and CS (20 - 25 GPa at a load of 413 kN/m). The comparable range of $\partial\sigma_y/\partial\varepsilon_y$ means that despite of the different overall compression and conductor layout, the

final stiffness is similar for these Nb_3Sn conductors and determined by the transverse stiffness of the Nb_3Sn strands.

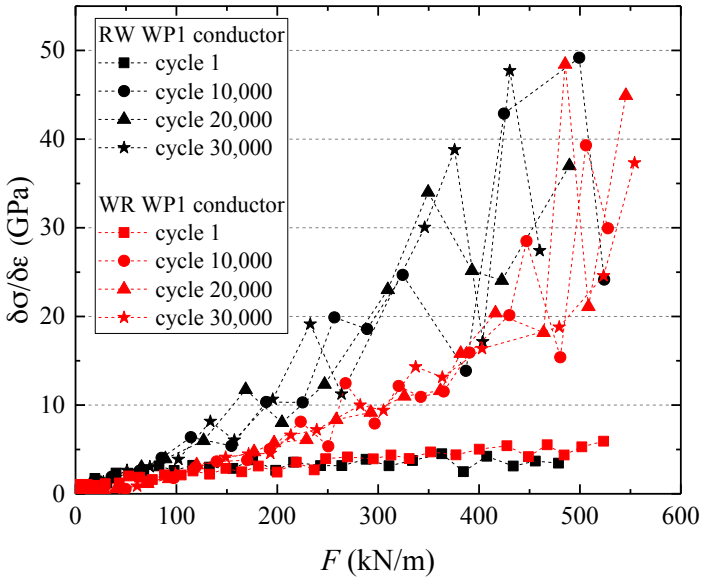

Figure 18. Dynamic elastic modulus for RW WP1 and WR WP2 samples upon increase of the load.

4. Conclusions

Two prototype TF conductors for the future EU DEMO reactor, with different desingns, were tested at the University of Twente in virgin condition and under transverse cyclic load.

The AC loss of the virgin samples was measured with the applied magnetic field orientation perpendicular and parallel to the wide side of the conductor. Both tested DEMO conductors showed high AC coupling loss while the hysteresis loss is on the same level as the ITER TF conductors. The RW WP1 conductor shows lower coupling loss than the WR WP2 conductor. Taking into account that both conductors were tested without any additional handling after heat treatment (i.e. like wind and react route) we can consider the AC coupling loss of the RW WP1 sample as an upper limit while the actual AC coupling loss will be lower after coil manufacturing. At the same time the measured AC coupling loss of the WR WP2 sample represents the coupling loss that might be expected after the magnet winding since the WR WP2 conductor follows the wind and react route.

The cyclic loading results in a change of the AC loss, contact resistance and mechanical properties though the effect is mitigated due to the low void fraction in comparison with ITER

TF conductors. The main changes in the coupling loss, contact resistance and mechanical properties take place up to 3,000 cycles. Although the AC coupling loss of both samples decreases with cycling of the load, the coupling loss time constant stays at a relatively high level, which is also explained by the low void fraction. After 30,000 cycles, the coupling loss time constant stays in the range of seconds for RW WP1 and tens of seconds for WR WP2.
Both conductors have interstrand contact resistance in the order of ~3 nΩm in the virgin state and this increases by a factor two after 30,000 cycles. The impact of cycling load on the contact resistances is more pronounced in the RW WP1 conductor.
Both conductors have a small mechanical deformation under the load, which again can be explained by the small void fraction. The displacement of the DEMO RW and WR samples is ~8 times smaller compared with the average displacement observed for ITER TF conductors. That results in small mechanical heat production during cycling of the load and is negligible compared with the AC losses in the measured DEMO conductors.

Acknowledgement

This work has been carried out within the framework of the EUROfusion Consortium and has received funding from the Euratom research and training programme 2014-2018 under grant agreement No 633053. The views and opinions expressed herein do not necessarily reflect those of the European Commission.

References

1. P. Bruzzone, K. Sedlak, B. Stepanov, R. Wesche, L. Muzzi, M. Seri, L. Zani, and M. Coleman, Design, Manufacture and Test of a 82 kA React&Wind TF Conductor for DEMO/IEEE TRANSACTIONS ON APPLIED SUPERCONDUCTIVITY, VOL. 26, NO. 4,4801805, JUNE 2016
2. Luigi Muzzi, Luigi Affinito, Sandro Chiarelli, Valentina Corato, Antonio della Corte, Aldo Di Zenobio, Rosa Freda, Simonetta Turtu`, Alessandro Anemona, Riccardo Righetti, Albano Bragagni, Massimo Seri, Fabio Gabiccini, Guido Roveta, Antonio Aveta, Stefano Galignano, Pierluigi Bruzzone, Kamil Sedlak, Boris Stepanov, and Rainer Wesche, Design, manufacture and test of an 80 kA-class Nb3Sn cable-in-conduit conductor with rectangular geometry and distributed pressure relief channels/IEEE TRANSACTIONS ON APPLIED SUPERCONDUCTIVITY, VOL. 27, NO. 4, 4800206, JUNE 2017
3. Pierluigi Bruzzone, Kamil Sedlak, Davide Uglietti, Nikolay Bykovsky, Luigi Muzzi, Gainluca De Marzi, Giuseppe Celentano, Antonio della Corte, Simonetta Turtù, Massimo Seri, LTS and HTS high current conductor development for DEMO/*Fusion Engineering and Design*,Volumes 96–97, October 2015, Pages 77–82
4. M. Kovari, R. Kemp, H. Lux, P. Knight, J. Morris, D.J. Ward, "PROCESS": A systems code for fusion power plants—Part 1: Physics/Fusion Engineering and Design 89 (2014) 3054–3069
5. P. Bruzzone, K. Sedlak, B. Stepanov, High current superconductors for DEMO, Fusion Eng. Des. 88 (9–10) (2013) 1564–1568.
6. L. Zani, C. M. Bayer, M. E. Biancolini, R. Bonifetto, P. Bruzzone, C. Brutti, D. Ciazynski, M. Coleman, I. Duran, M. Eisterer, W. H. Fietz, P. V. Gade, E. Gaio, F. Giorgetti, W. Goldacker, F. Gömöry, X. Granados, R. Heller, P. Hertout, C. Hoa, A. Kario, B. Lacroix, M. Lewandowska, A. Maistrello, L. Muzzi, A. Nijhuis, F. Nunio, A. Panin, T. Petrisor, J.-M. Poncet, R. Prokopec, M. Sanmarti Cardona, L. Savoldi, S. I. Schlachter, K. Sedlak, B. Stepanov, I. Tiseanu, A. Torre, S. Turtù, R. Vallcorba, M. Vojenciak, K.-P. Weiss, R. Wesche, K. Yagotintsev, and R. Zanino, Overview of Progress on the EU DEMO ReactorMagnet System Design/ IEEE TRANSACTIONS ON APPLIED SUPERCONDUCTIVITY, VOL. 26, NO. 4, 4204505, JUNE 2016
7. Hamada K, Takahashi Y, Matsui K, Kato T and Okuno K 2004 Effect of electromagnetic force on the pressure drop and coupling loss of a cable-in-conduit conductor *Cryogenics* **44** 45
8. A. Nijhuis, N. W. Noordman, O. A. Shevchenko, H. J. ten Kate, and N. Mitchell, "Electromagnetic and mechanical characterization of ITER CS-MC conductors

affected by transverse cyclic loading, part 3: Mechanical properties," *IEEE Trans. Appl. Supercond.*, vol. 9, pp. 165–168, 1999.
9. A. Nijhuis and Y. Ilyin, "Transverse cable stiffness and mechanical losses associated with load cycles in ITER Nb3Sn and NbTi CICCs," *Supercond. Sci. Technol.*, vol. 22, p. 055007, 2009.
10. A. P. Verweij, "Electrodynamics of superconducting cables in accelerator magnets", ISBN 90-9008555-6 (1995).
11. Abbas W, Nijhuis A, Ilyin Y, ten Haken B and ten Kate H H J 2004 A fully automatic press for mechanical and electrical testing of full size ITER conductors under transverse cyclic load Adv. Cryog. Eng.Mater. 50 51–8
12. Nijhuis, N. W. Noordman, H. J. ten Kate, N. Mitchell, and P. Bruzzone, "Electromagnetic and mechanical characterization of ITER CS-MC conductors affected by transverse cyclic loading, part 1: Coupling current loss," *IEEE Trans. Appl. Supercond.*, vol. 9, pp. 1069–1072, 1999.
13. A. Nijhuis, N. W. Noordman, H. J. ten Kate, N. Mitchell, and P. Bruzzone, "Electromagnetic and mechanical characterization of ITER CS-MC conductors affected by transverse cyclic loading, part 2: Interstrand contact resistances," *IEEE Trans. Appl. Supercond.*, vol. 9, pp. 754–757, 1999.
14. A. Nijhuis, Y. Ilyin, W. Abbas, B. ten Haken, and H. H. J. ten Kate, "Change of interstrand contact resistance and coupling loss in various prototype ITER NbTi conductors with transverse loading in the Twente Cryogenic Cable Press up to 40,000 cycles," *Cryogenics*, vol. 44, pp. 319–339, 2004.
15. A. Nijhuis, Y. Ilyin, W. Abbas, H. H. J. ten Kate, M. V. Ricci, and A. della Corte, "Impact of void fraction and evolution of coupling loss in ITER Nb3Sn conductors under cyclic load," *IEEE Trans. Appl. Supercond.*, vol. 15, pp. 1633–1636, 2005.
16. Y. Miyoshi, Y. Ilyin, W. Abbas, and A. Nijhuis "AC Loss, Inter-Strand Resistance, and Mechanical Properties of an Option-II ITER CICC up to 30,000 Cycles in the Press"IEEE TRANSACTIONS ON APPLIED SUPERCONDUCTIVITY, VOL. 21, NO. 3, JUNE 2011
17. Yagotintsev W.A.J. Wessel, A. Vostner, A. Devred, D. Bessette, N. Mitchell, Y. Nabara, T. Boutboul, V. Tronza, S.-H. Park, W. Yu, N. Martovetsky and A. Nijhuis, Overview of verification tests on AC loss, contact resistance and mechanical properties of ITER conductors with transverse loading up to 30,000 cycles / send for publication to SUST 2017
18. A. Nijhuis, H. H. J. ten Kate, P. Bruzzone, and L. Bottura, "Parametric study on coupling loss in subsize ITER Nb_3Sn cabled specimen", IEEE Trans. Magn. 32, 2743 (1996).
19. Takahashi Y, Matsui K, Nishii K, Koizumi N, Nunoya Y, Isono T, Ando T, Tsuji H, Murase S, Shimamoto S 2001 AC Loss Measurement of 46 kA-13T Nb3Sn Conductor for ITER, *IEEE Trans. Appl. Supercond.***11** 1546-1549

20. M.D. Sumption, R.M. Scanlan and E.W. Collings, AC loss properties of some Bi:2212/Ag Rutherford cables and a comparison with those of cables wound with NbTi and Nb3Sn/ Cryogenics 38 (1998) 1225–1232
21. N. Wilson, A.K. Ghosh, B. ten Haken, W.V. Hassenzahl, J. Kaugerts, G. Moritz, C. Muehle, A. den Ouden, R. Soika, P. Wanderer, W. A. J. Wessel, Cored Rutherford Cables for the GSI Fast Ramping Synchrotron/ Presented at tlie Applied Superconductivity Conference at Houston, TX , August 4-9,2002